PCCP

Accepted Manuscript




ROYAL SOCIETY OF CHEMISTRY

www.rsc.org/pccp

# Phase evolution and electrical properties of Co-Sb alloy fabricated from Co/Sb bilayers by thermal annealing and ion beam mixing

*Manju Bala [a*], Compesh pannu[a], Srashti Gupta [a], Tripurari. S. Tripathi [b], Surya K. Tripathi [c], K. Asokan [a*] and Devesh K. Avasthi [a]*

[a] Inter-University Accelerator Centre, Aruna Asaf Ali Marg, New Delhi-110067, India

[b] Aalto University, Värmemansgränden 2, 02150 Esbo, Finland

[c] Department of Physics, Panjab University, Chandigarh-160 014, India

**Abstract:**

An investigation was carried out to understand the phase evolution and study the structural, morphological, optical and electrical properties of Co-Sb alloy fabricated by two different approaches:(a) Thermal annealing and (b) Ion-beam mixing followed by post annealing. The as-deposited and 100 MeV Ag ion beam irradiated Co/Sb bilayer thin films were subjected to thermal annealing from 200 to 400$^{o}$C for 1 hour. The Rutherford backscattering spectrometry (RBS) results showed partial mixing for thermally annealed films while complete mixing for irradiated and post annealed films at 400$^{o}$C. The XRD and RAMAN measurements indicated the formation of Co-Sb alloy, having ~ 70% concentration of $CoSb_3$ phase in the irradiated post annealed sample at 400$^{o}$C. Band gap of the annealed and post irradiated annealed Co-Sb alloy were determined from UV-visible spectroscopy. The electrical and thermoelectric power measurements were done in the temperature range of 300-420 K. It was observed that alloy formed by ion-beam induced mixing exhibit higher electrical conductivity and thermoelectric power compared to the as-deposited and thermally annealed Co/Sb bilayer thin films.

**Key words:** Skutterudite, Ion beam induced mixing, Phase evolution, Thermoelectric Power

## Introduction

Under skutterudite family cobalt-antimony based compounds possess a history of research inspired by their unique thermoelectric properties near mid temperature range[1-2] (400-900K). It has been found that Co-Sb compounds under a stoichiometric ratio of 1:3 give best

thermoelectric performance[3]. Thermoelectric efficiency (Z) of a material is given by $S^2/\rho\kappa$, where $S$ is the Seebeck coefficient (thermoelectric power), ρ is electrical resistivity and κ is the thermal conductivity. Thermoelectric efficiency depends on stoichiometric composition, surface morphology, material defects, etc. For good microthermoelectric devices thin film having large thermoelectric power with lower electrical resistivity and thermal conductivity are essential[4]. Unfortunately, thermal conductivity of the binary skutterudites is too large for thermoelectric applications. It was found that structural modification of these compounds, i.e. doping them with heavy atoms or making mixed crystals of skutterudites greatly improves their thermoelectric properties[5-7]. Filled skutterudites exhibit lower thermal conductivity due to enhanced phonon scattering[8]. Various groups have prepared thin films of Co-Sb alloys by RF co-sputtering, magnetron dc sputtering, pulsed laser deposition (PLD), spark plasma sintering, and molecular beam deposition (MBD)[9-13]. Ahmed et al fabricated the Co–Sb thin films with Sb content in the range of 65–76 at.% by RF co-sputtering and found maximum power factors of 0.73 $mWm^{-1}$ $K^{-2}$ and 0.67 $mWm^{-1}$ $K^{-2}$ for the $CoSb_2$ and $CoSb_3$ thin films, respectively[9]. $CoSb_3$ films were prepared by Savchuk *et al.* on oxidized Si and ceramic $Al_2O_3$ substrates using magnetron dc sputtering technique and found the Seebeck coefficient of -250 μV/K at ~ 550 K for both substrates[10] . In and Yb-doped $CoSb_3$ thin films prepared by PLD method resulted in the Seebeck coefficient nearly -150μV/K at about 700 K[11]. Recently, Daniel *et al.* synthesized Co–Sb thin films by MBD at different substrate temperatures as well as on non-heated substrates followed by a post-annealing. Extended investigation of the phase formation with dependence on deposition method and parameters[12]. Dong *et al.*, prepared Se and Te/Se-doped *n*-type $CoSb_3$ skutterudites by high-pressure synthesis (HPS) followed by spark plasma sintering and found that the highest *ZT* value of 1.29 is achieved at 780 K for $CoSb_{2.8}Te_{0.15}Se_{0.05}$ with an appropriate Te/Se co-doping[13].

The ion beam processing of materials is one of the novel methods of synthesis of thin films of thermoelectric materials. Ion beam mixing provides an important means of alloy formation with creation of defects and nanostructures in the material which have been reported to result in the enhancement of Seebeck coefficient and lowering of the thermal conductivity by carrier energy filtering and phonon scattering, respectively. Srashti *et al.* reported that PbTe synthesized by ion beam mixing of Te/PbO bilayer leads to the formation of nanostructures on the surface[14].

Ibrahim *et al.*[15] found that Bi-Sb alloys thin films of various compositions can be prepared by ion beam mixing. They reported the formation of $Bi_{87}Sb_{13}$ alloy by irradiating Bi/Sb with 120 keV $Kr^+$ at a fluence of $7\times10^{15}$ ions/cm$^2$ and showed an increase of about 30% in *ZT* over that of pure Bi. Beneson *et al.*[16] showed that Bi-Te alloy formed by ion beam mixing of Bi/Te alloy using 130keV Xe ion have maximum thermopower (55μV/K) at a fluence of $8\times10^{15}$ $Kr^+$/cm$^2$. The ions having energies ~ a few MeV/amu, called swift heavy ions (SHI), on their passage through any material, deposit large amounts of energy (tens of keV/nm) via inelastic collisions in the electronic subsystem of the lattice. This is termed as electronic energy loss, $S_e$. In this case, the energy lost by the incident ion due to interaction with nuclei (called, nuclear energy loss or $S_n$) is usually negligible. Above a certain $S_e$ threshold, the electronic excitations induce atomic displacements in a majority of materials, which can lead to mixing of two components of a binary system[17]. SHI irradiation can produce defects at the bilayer interface. Thereafter, rearrangement of the interfacial atoms and short-range diffusion can cause mixing of the two components. In some cases, the latter is enhanced by post irradiation annealing[18 19], during which nucleation and phase growth can occur. Bhattacharya *et al.*[20] reported that SHI irradiation (120 MeV Au) followed by vacuum annealing, induce modification of the Co (60 nm)/Si interface. A uniformly mixed region constituting crystalline phases of cobalt silicides was formed after heat treatment (>400$^o$C) of irradiated samples.

It has been reported that it is possible to increase the thermoelectric figure of merit (*ZT*) of certain materials by preparing them in the form of two-dimensional structures. Hicks *et al.* prepared PbTe/$Pb_{1-x}Eu_xTe$ multiple-quantum-well (MQW) structures by molecular-beam epitaxy and performed thermoelectric and other transport measurements as a function of quantum-well thickness (17 and 55 Å). *ZT* value were found to be higher than the bulk values which may be possible through quantum confinement effects using quantum-well structures[21]. Venkatasubramanian *et al.* reported that thin film thermoelectric materials demonstrate a significant enhancement in *ZT* at 300 K, compared to state-of-the-art bulk $Bi_2Te_3$ alloys. Such an enhancement was achieved by controlling the transport of phonons and electrons in the superlattices[22]. Present study aims to synthesize $CoSb_3$ alloy thin films using thermal annealing and radiation enhanced mixing of Co/Sb bilayer thin film system by high energy heavy ion beam. It is known that bilayer mixing of thin films results in nanostructuring[23] which improves

thermoelectric properties[24-25]. Ion beam induced mixing leads to alloy formation at the interface and results in defect creation which may lower the lattice thermal conductivity by phonon scattering. Moreover, the ion beam induced mixing technique of sample preparation was used as it provides a control over mixing and phase formation. In this study, the structural evolution of different phases of cobalt antimonide with different ion beam parameters and annealing temperature and their effects on thermoelectric properties of Co/Sb bilayer thin film were investigated.

**Experimental Details**

Co/Sb bilayer thin films were synthesized by electron beam evaporation of cobalt on cleaned quartz substrates followed by thermal evaporation of Sb under the pressure of $10^{-5}$ torr at room temperature at Panjab University, Chandigarh. The initial choice of film thickness for Co and Sb were Co(50nm)/Sb(150nm). This layer thickness was chosen in order to keep equal number of Co and Sb atoms in the two layers. The atomic density of Co and Sb are $9.09\times10^{22}$ atoms/cm$^3$ and $3.31\times10^{22}$ atoms/cm$^3$ respectively, therefore 50 nm of Co and 150 nm of Sb have nearly same number of atoms (~$5\times10^{17}$ atoms/cm$^2$). However, Rutherford Backscattering Manipulation Program (RUMP) simulation of Rutherford backscattering spectrometry (RBS) data showed that the initial thickness of bilayer which got deposited was Co(57nm)/Sb(163nm).

These bilayer films were irradiated by 100 MeV $Ag^{7+}$ ions with 1 pnA ion current (pnA stands for particle nA and is equal to current in nA divided by charge state of the ion used) with two different fluence $5\times10^{13}$ and $1\times10^{14}$ ions/cm$^2$ using a 15-UD pelletron facility at Inter-University Accelerator Centre (IUAC), New Delhi. The irradiation was carried out at room temperature and pressure was maintained at $10^{-6}$ torr. For uniform irradiation, the focused beam was allowed to scan over an area of 1 x 1 cm$^2$. The as-deposited and irradiated films were annealed for 1 hour in the atmosphere of Ar+$H_2$ at 200, 300 and 400$^o$ C in the tubular furnace. It may be noted that the melting point of Sb is 630$^o$C and hence the maximum annealing temperature was restricted to 400$^o$C.

For convenience hereafter, the pristine as-deposited Co/Sb bilayer thin films will be referred as P; the films annealed from 200 to 400$^o$C as $A_{200}$, $A_{300}$ and $A_{400}$; the $5\times10^{13}$ and $1\times10^{14}$

irradiated samples as $I_{5e13}$ and $I_{1e14}$; and irradiated post annealed samples at 200 to 400$^{o}$C as $IA_{200}$, $IA_{300}$ and $IA_{400}$. Rutherford backscattering spectrometry RBS was performed using 1.7 MV tandem accelerator facility with 2 MeV $He^{+}$ ions at scattering angle of 165$^{o}$ at IUAC, New Delhi for compositional and depth profile studies of P, A, I and IA samples. The data were analyzed using Rutherford Universal Simulation Program (RUMP)[26]. XRD measurements of all the samples were carried out on Indian beam line BL – 18B, at synchrotron facility, Photon Factory, Tsukuba. The conventional XRD did not provide intense, sharp and well resolved data due to limited resolution and low photon intensity, and very small thickness of the thin films. Therefore the XRD measurement were performed using synchrotron facility at Photon Factory, KEK Japan where high energy intense X-rays are available and gives better resolution. This measurement is not expected to cause any damage to these compounds. HRXRD measurements were carried out with Bragg Brentano diffractometer at a glancing angle of 2$^{o}$ using 13.6 keV photon in the 2θ scan region of 15$^{o}$-45$^{o}$. Raman spectroscopy was performed using an Invia microRaman setup from Renishaw. Ar ion laser of wavelength 514 nm, laser power 5 mW and exposure time of 40 s was used in the measurement. The peak intensities are obtained by Lorentzian fitting process assuming Lorentzian distribution. The study of the changes in optical properties was carried out by recording UV–visible absorption spectra using the unpolarized dual beam Hitachi U3300 spectrophotometer in the spectral range 200–800 nm. The surface morphology of thin films were examined by field emission scanning electron microscopy (FESEM) [MIRA II,TESCAN] using electron beam of energy 20keV and Nanoscope IIIa, atomic force microscopy (AFM) in tapping mode. Electrical conductivity (σ) and thermoelectric power (S) of these films were measured as a function of temperature in the range from 300 to 400 K using four probe and bridge method[27], respectively. The Hall Effect measurements were carried out using a magnetic field of 0.57 Tesla at room temperature to evaluate carrier density and mobility.

## Results and Discussion

### Compositional study

The RBS spectra of bilayer films irradiated with 100 MeV Ag ions at fluences $5\times10^{13}$ and $1\times10^{14}$ ions/cm$^{2}$ and post annealed at 400$^{o}$C for 1 hour, indicate that mixing take place to a greater

extent in case of the films irradiated at a fluence of $1\times10^{14}$ ions/cm$^2$. Therefore, for further detailed studies only the films irradiated at $1\times10^{14}$ ions/cm$^2$ fluence were taken into consideration. The RBS spectra of P, $I_{1e14}$, $IA_{200}$, $IA_{300}$ and $IA_{400}$ samples are shown in figure 1. RBS spectrum of bilayer film P comprises of two well resolved peaks corresponding to Co and Sb. Within the resolution limit of RBS technique there is no significant change in the spectra of $I_{1e14}$ samples in comparison to the pristine bilayer thin film sample. Figure 1 shows that for irradiated samples mixing start at annealing temperature of about 200$^o$C and mixing increases on further increasing the annealing temperature to 400$^o$C. As Co peak moves toward high energy side and Sb towards low energy side, these imply that Co atoms are diffusing towards the surface and Sb atoms into the Co layer. There is complete and uniform mixing of Co and Sb layers for $IA_{400}$ thin films. Figure 2 shows the RBS spectra of P, $A_{400}$ and $IA_{400}$ thin films. The distinction between the effects of annealing and irradiation followed by annealing lies on the uniformity of mixing. The flat plateau in Co peaks of $IA_{400}$ sample in comparison to the hump in Co peak of $A_{400}$ sample shows that there is more uniform mixing in $IA_{400}$ sample for the same annealing temperature. The RBS spectra of P, $A_{400}$ and $IA_{400}$ were fitted and the depth profiles were extracted using the Rutherford Backscattering Manipulation Program (RUMP) simulation code as shown in Figure 3. The simulations show that for P sample thickness of Sb layer is ~163 nm followed by a ~57 nm thick Co layer. There is a shift of Co peak towards high energy side and a reduction of peak intensity of both Co and Sb for both $A_{400}$ and $IA_{400}$ thin film samples. For $A_{400}$ sample (figure3(b)), mixing is observed however it is not uniform throughout the film. $A_{400}$ sample has a top layer of~110nm thick having concentration of Sb~52 to 61%, Co~20 to 30% and O~18% followed by 67 nm thick layer having Sb~50 to 53%, Co~41 to 44% and O~5%.. For $IA_{400}$ sample there is uniform mixing of Co and Sb layers through a thickness of 177 nm having Sb~52%, Co~28 to 32% and O~17 to 20% (figure 3(c)). RBS provides information only about the elemental composition in a particular thickness and not on the details about the chemical formula, phase or alloy formed. The presence of oxygen in the mixed layer of $IA_{400}$ sample (as shown in depth profiling) does not confirm that oxygen is present in the form of oxides of Co, Sb or CoSb. XRD shows the presence of $Sb_2O_3$ only for A, $IA_{200}$, $IA_{300}$ samples where some antimony oxide is formed and no $Sb_2O_3$ peak is detected for IA400 sample (figure 4(a-b)), therefore one can assume that in case of $IA_{400}$ sample all oxygen is located at the grain

boundaries without forming any oxide with Sb. This may be due to the greater tendency of Sb at this temperature to form alloy with Co rather than Oxygen.

Interdiffusion of Co and Sb that occurs during annealing of irradiated sample can possibly be explained as follows. SHI generates defects on either side of the interface, on its passage through the material. These defects are largely immobile and it is only after the thermal energy supplied to the system during the annealing processes that the atomic mobility occurs through these defects, and across the interface, is enhanced leading to the uniform mixing of the two layer.

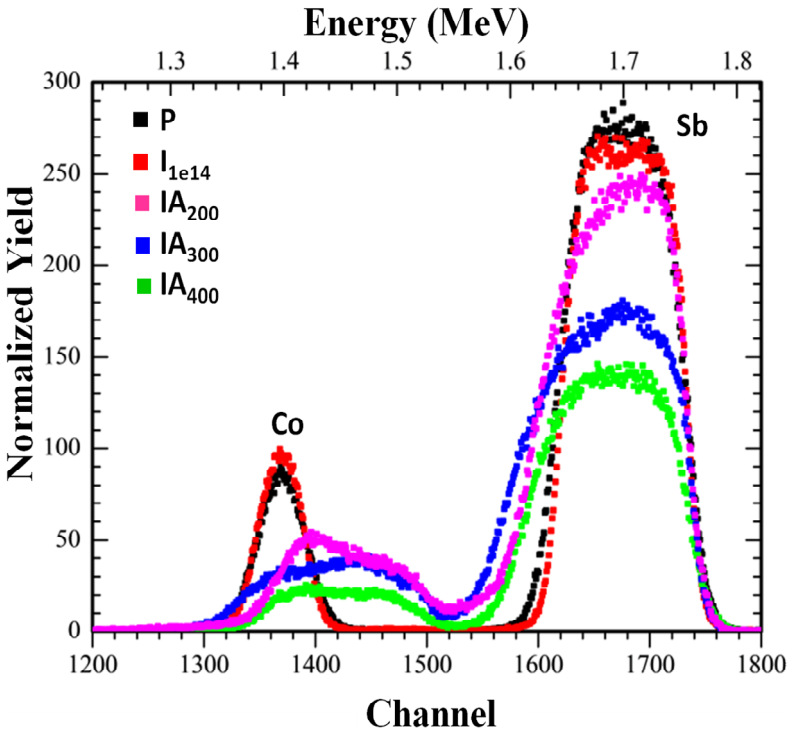


Figure 1: Comparison of RBS data corresponding to P, I, $IA_{200}$, $IA_{300}$, $IA_{400}$ Co/Sb bilayer thin films. Maximum mixing observed for $IA_{400}$.

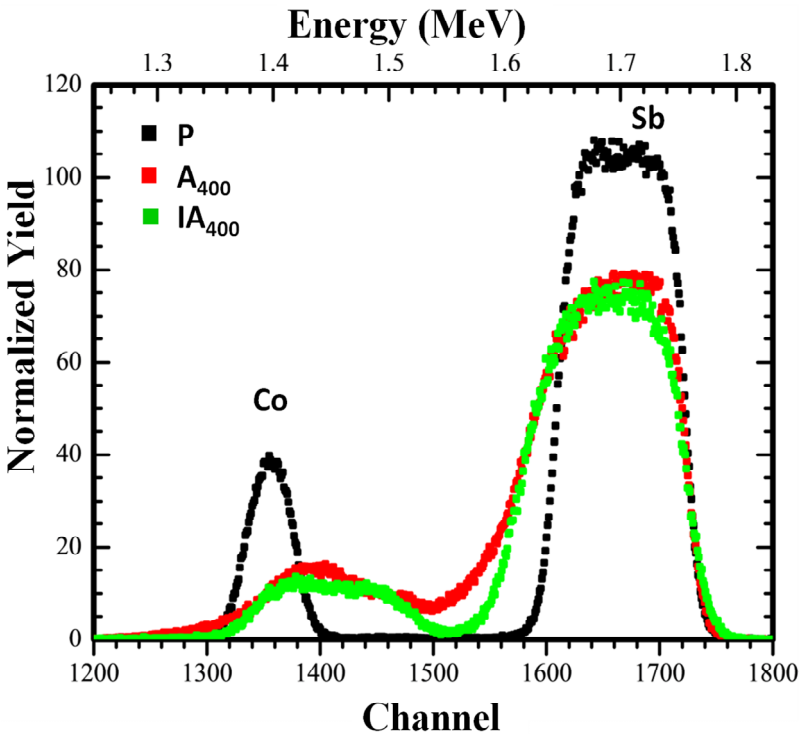


Figure 2: RBS spectra of the P, $A_{400}$, $IA_{400}$ Co/Sb bilayer thin films. Complete and uniform mixing observed for $IA_{400}$.

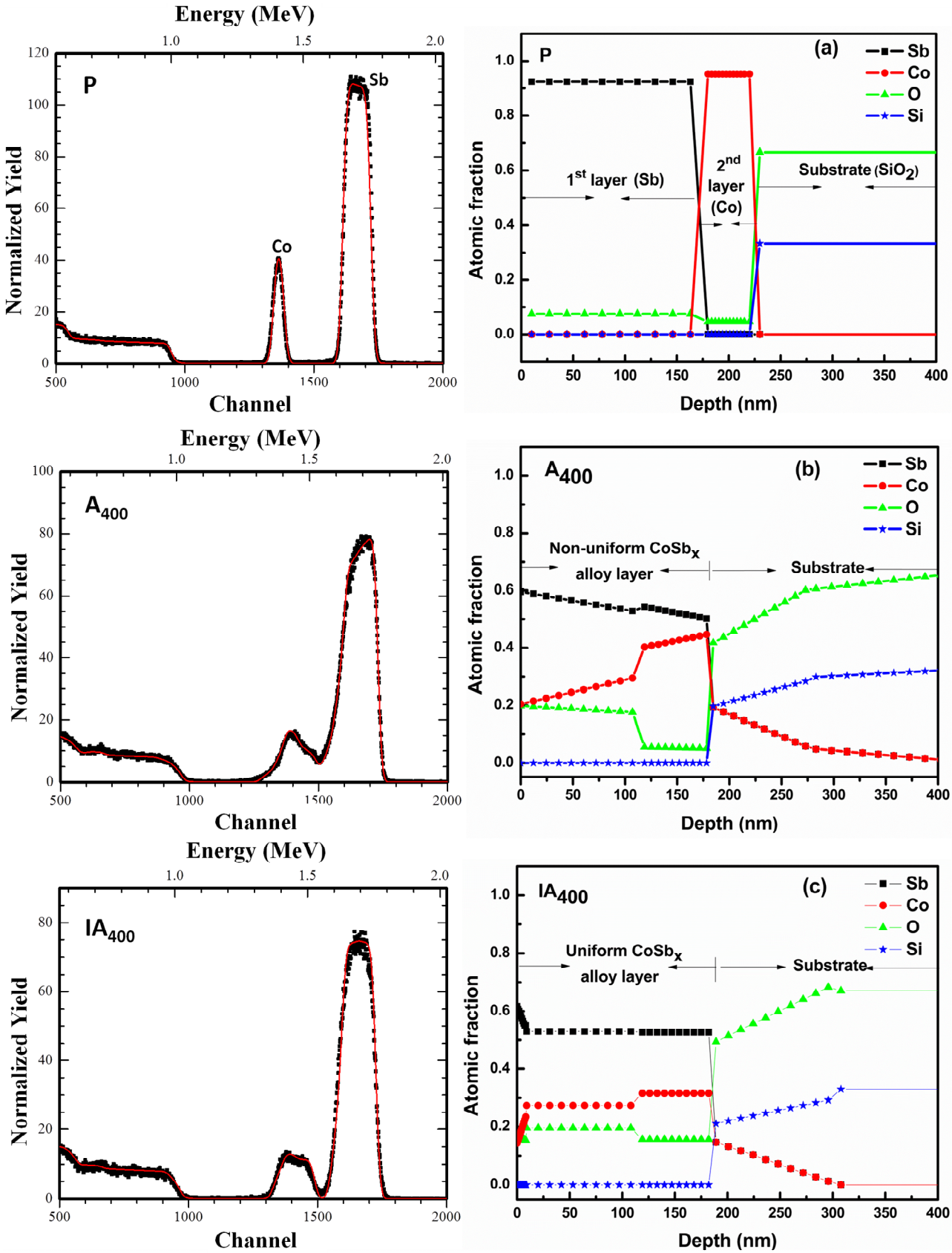

Figure 3: RBS fitted spectra and corresponding depth profiles extracted from RBS analysis of (a) P (b) $A_{400}$ and (c) $IA_{400}$ bilayer Co/Sb thin film. uniform mixing observed for $IA_{400}$.

**High Resolution XRD**

Figure 4 shows HRXRD spectra of (a) P, $A_{200}$, $A_{300}$ and $A_{400}$ thin films and (b) P, $IA_{200}$, $IA_{300}$ and $IA_{400}$ thin films. The XRD spectrum of P sample shows peaks corresponding to Sb only which is present as a top layer. $A_{200}$ and $A_{300}$ samples show peaks corresponding to Sb and $Sb_2O_3$ phase *(JCPDS85-1324),(JCPDS26-0101), (JCPDS02-0592), (JCPDS11-0689)* indicating the oxidation of Sb during annealing, while $A_{400}$ film show peaks corresponding to CoSb *(JCPDS33-0097)*, $CoSb_2$ *(JCPDS29-0126)* and $CoSb_3$ phases *(JCPDS83-0055)* (figure 4(a)). For bilayer thin films irradiated with 100 MeV Ag ions at $1\times10^{14}$ ions/cm$^2$ fluence, no phase change was observed and all the XRD peaks were corresponding to Sb only therefore it is not shown in the figure, however for $IA_{300}$ and $IA_{400}$ peaks corresponding to Co-Sb alloy appears. XRD spectrum of $IA_{200}$ sample shows peaks that correspond to phases of Sb and $Sb_2O_3$. While the $IA_{300}$ sample shows the phases of Sb, $Sb_2O_3$, $CoSb_2$ and $CoSb_3$, the $IA_{400}$ samples has only the peaks corresponding to $CoSb_2$ and $CoSb_3$ phases. This shows that, Co-Sb phase is formed at much lower annealing temperature (300$^o$C) in the irradiated samples in comparison to the just annealed samples where Co-Sb alloy phase appears only at 400$^o$C. Compositions of different Co-Sb phases for $IA_{400}$ and $A_{400}$ films are given in table 1. Comparing the areal concentration of different phases of Co-Sb it is found that in case of $IA_{400}$ samples concentration of $CoSb_3$ phase is 17 % higher than $A_{400}$ sample.

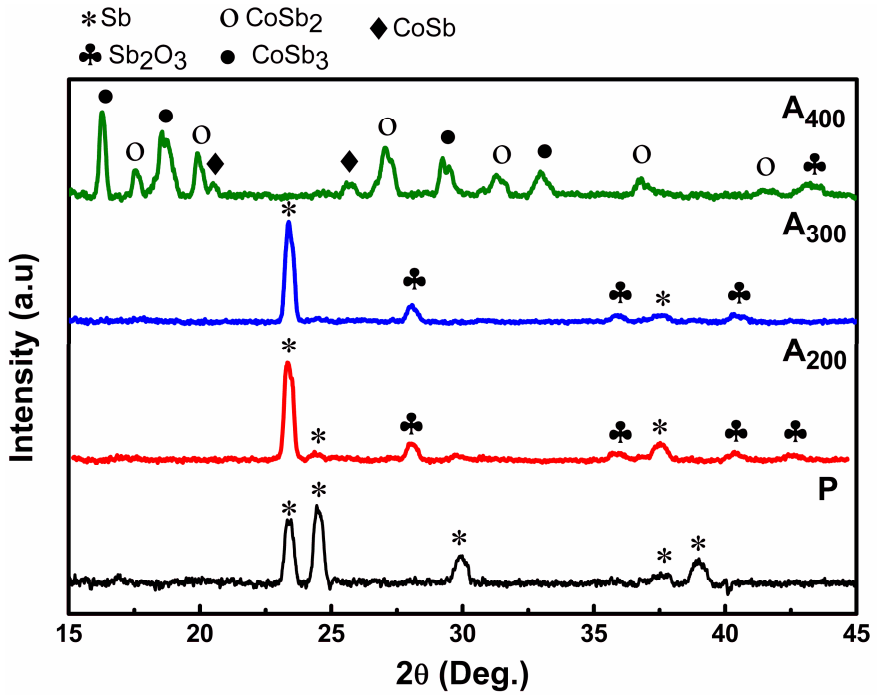


(a)

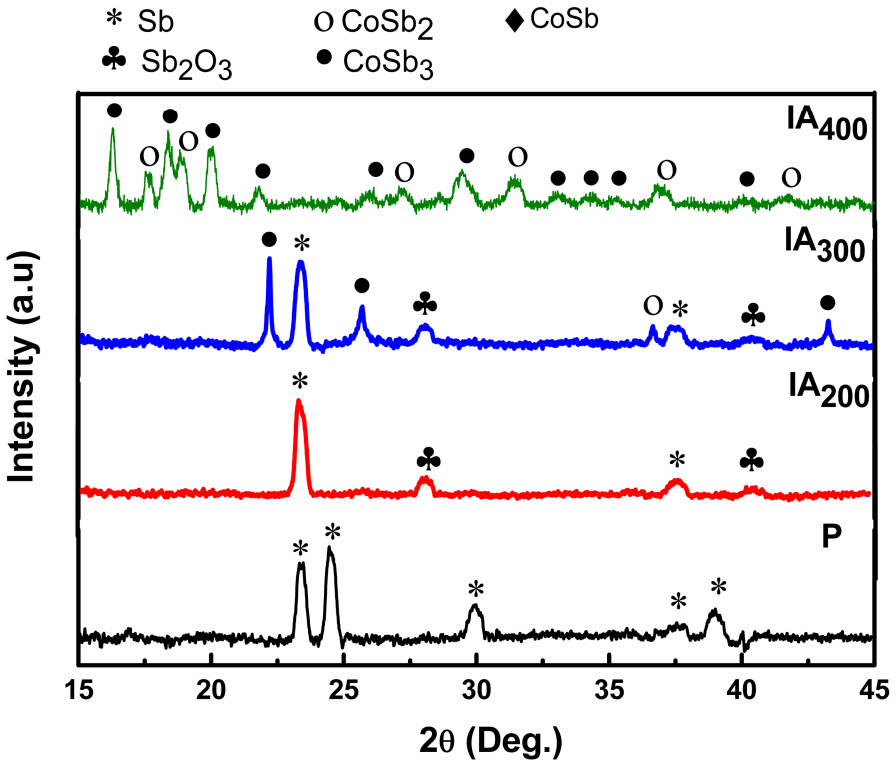


(b)

Figure 4: HRXRD spectra of (a) P, $A_{200}$, $A_{300}$, and $A_{400}$ (b) P, $IA_{200}$, $IA_{300}$, and $IA_{400}$ Co/Sb bilayer thin film. Note that the phases of $CoSb_2$ and $CoSb_3$ are observed in $IA_{400}$ film.

Table 1: Areal concentrations of different phases in $IA_{400}$, and $A_{400}$ thin films.

| | **$Sb_2O_3$** | **CoSb** | **$CoSb_2$** | **$CoSb_3$** |
|---|---|---|---|---|
| **Annealed at 400°C ($A_{400}$)** | 6% | 7% | 34% | 53% |
| **Irradiated annealed at 400°C ($IA_{400}$)** | 0% | 0% | 30% | 70% |

**Raman Spectroscopy**

The Raman spectra of the P, $A_{400}$, and $IA_{400}$ Co/Sb thin films are shown in figure 5. The spectrum for P sample shows characteristic peaks at 188 $cm^{-1}$ (F2g), 252$cm^{-1}$(A1g) for $Sb_2O_3$ which fit well with the data of Zeng et al.[28] (187.5 and 251.5 $cm^{-1}$). In addition there arises a peak at 149.8 $cm^{-1}$ which by group-theory analysis is shown to be A1g mode for Sb [29]. In $A_{400}$ the peaks evolves at 112.1 and 149.3 $cm^{-1}$ corresponding to F2g and A1g Raman active modes, these peaks shows a shift to 110.1 and 147.9 $cm^{-1}$ for $IA_{400}$ samples which are in well in agreement to the peak of skutterudite $CoSb_3$ (110$cm^{-1}$ f2g, 148 $cm^{-1}$ Ag1)[30-31]. Therefore a phase evolution of $CoSb_3$ can be observed as the peak at 149.8 $cm^{-1}$ (Sb) for P sample moves toward 147.9 $cm^{-1}$ ($CoSb_3$) for $IA_{400}$ sample. It is also seen from the spectra that the intensity of the peaks increases for $IA_{400}$ sample in comparison to $A_{400}$ sample due to increase in $CoSb_3$ concentration from 53% to 70%.

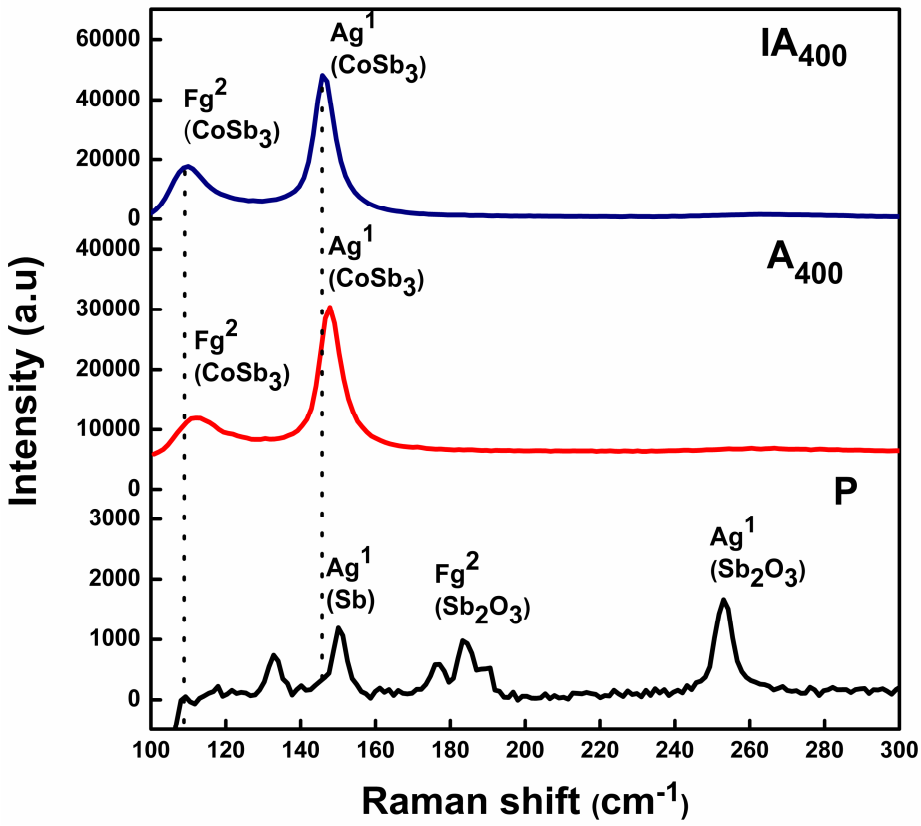


Figure 5: Raman spectra of P, $A_{400}$, and $IA_{400}$ thin films

**UV–visible absorption spectroscopy**

UV–visible spectroscopy is an important tool for optical characterization of materials. It provides useful information about the optical band gap of the semiconductors. The optical absorption study of the P, $A_{400}$, $IA_{400}$ Co/Sb films were carried out and the band gap of the films have been calculated using Tauc's plot by plotting $(\alpha h\nu)^r$ versus hν and extrapolating the linear portion of the absorption edge to find the intercept with energy axis. The P sample showed no absorption edge. The Tauc's plots of $A_{400}$ and $IA_{400}$ Co/Sb thin film are shown in figure 6(a-b), respectively. The estimated value of energy gap for $A_{400}$ sample is 2.4 eV which reduces to 0.89 eV for $IA_{400}$ sample. Here r =1/2, which is for direct band gap. This shows that $CoSb_3$ alloy is a direct band gap semiconductor. The shift in $E_g$ upon irradiation may be due to creation of intermediate energy levels[32], quantum confinement effect[33], increase of grain size[34]. In present case as found from the HRXRD spectra, the alloys formed in the $A_{400}$ sample are $Sb_2O_3$, CoSb, $CoSb_2$, $CoSb_3$ and that in $IA_{400}$ samples are $CoSb_2$ and $CoSb_3$. The band gap of $Sb_2O_3$ is 3.4 eV[35] and that of

Co-Sb alloys varies from 0.1-0.5 eV [36]. Therefore the shift in band gap from 2.7eV for $A_{400}$ sample to 0.89eV for $IA_{400}$ sample may be because of the greater percentage of Co-Sb alloy in $IA_{400}$ sample.

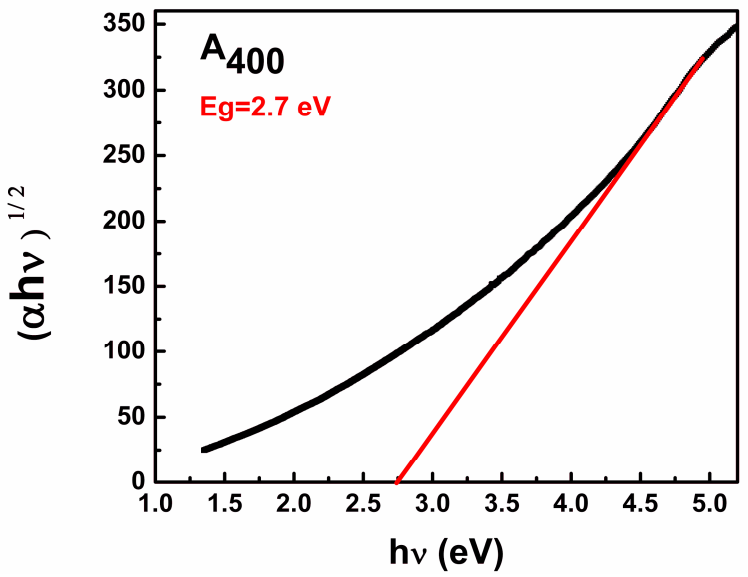


(a)

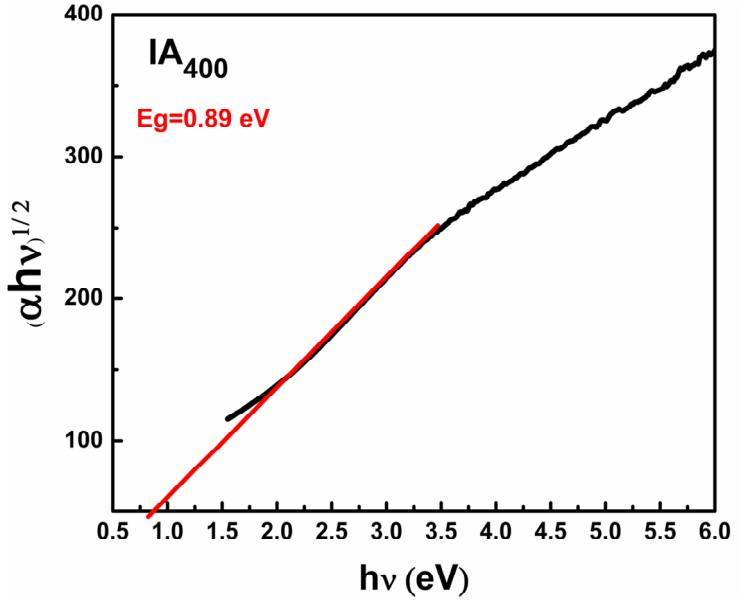


(b)

Figure 6: Tauc's plot of (a) $A_{400,}$ Co/Sb thin film samples band gap ~ 2.7eV and (b) $IA_{400}$ Co/Sb thin film samples, band gap ~ 0.89eV

**Morphological study**

Figure 7(a-c) shows FESEM images of the P, $A_{400}$, and $IA_{400}$ Co/Sb bilayer thin film, respectively. The surface of P film appears smooth and flat. A significant change in surface morphology of $A_{400}$ and $IA_{400}$ sample is found. For $IA_{400}$, rod like nanostructures that extends outward from a central point appears throughout the surface, for the $IA_{400}$ samples. The coral like structures shown in magnified image (figure 7(c2)) appear due to the impact of the Ag ion beam on the surface.

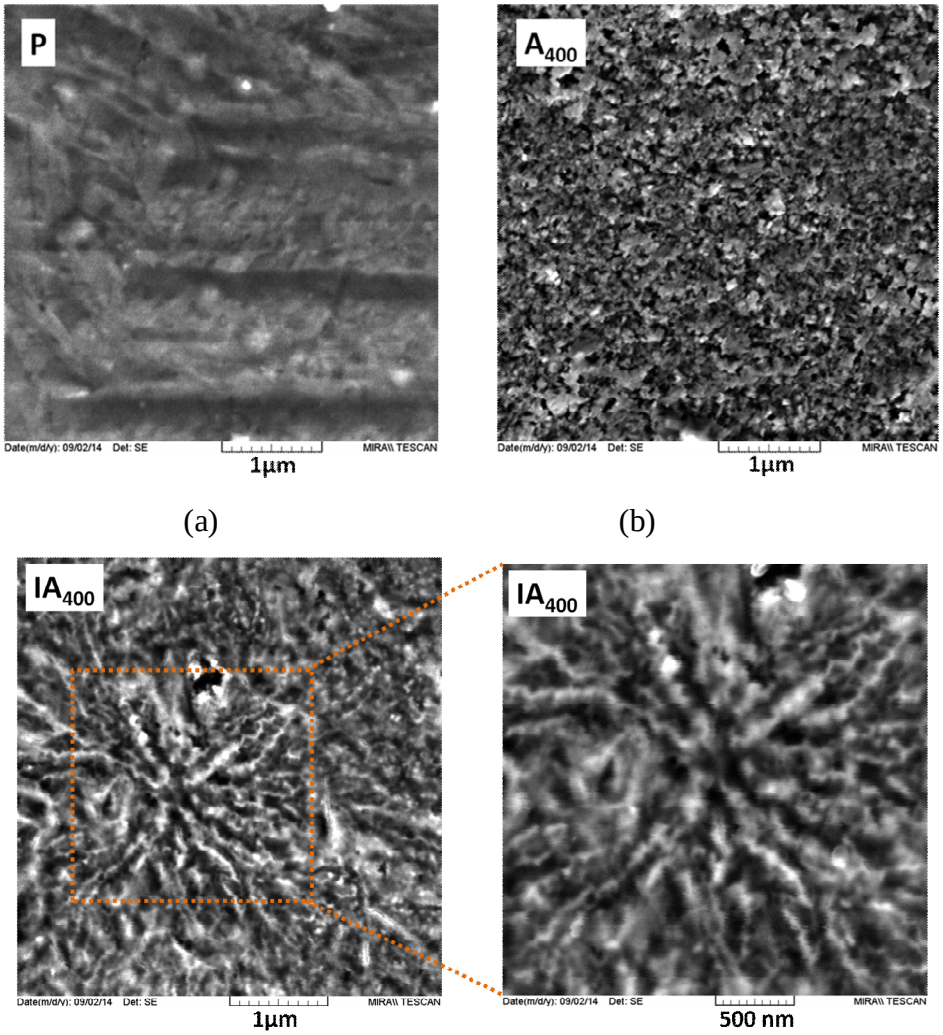


Figure 7: SEM images of (a) P, (b) $A_{400}$ and (c1) $IA_{400}$ sample and (c2) magnified image of $IA_{400}$

The AFM images of P, $A_{400}$, and $IA_{400}$ Co/Sb thin films are shown in figure 8(a-c). A change in surface morphology is clearly observed for $A_{400}$, $IA_{400}$ samples. The P film exhibits dense, smooth and flat surface. AFM shows that the root mean square (rms) surface roughness of the P sample is ~11.4 nm which on annealing at 400°C increases to ~ 65.6nm and to 76.8 nm on post irradiation annealing. In case of the pristine sample two thin film layers are deposited one over other. The rms roughness of as deposited pristine thin film was therefore less (~11.4 nm).

The $A_{400}$ sample was prepared by thermal annealing of pristine sample at 400°C. This annealing results in mixing of the bilayer film through diffusion of Co and Sb atoms across the interface. The diffusion of atoms leads to surface modification resulting in a rough surface as shown in the image. Therefore, due to migration of atoms through the interface into each other, the surface roughness of $A_{400}$ sample increases and is ~ 65.6 nm. The $IA_{400}$ sample was prepared by annealing the irradiated ($1\times10^{14}$ions/cm$^2$ fluence) sample at 400°C. Here the surface roughness is still higher (~76.8 nm) than the $A_{400}$ sample because of the defects created by ion beam irradiation in addition to the diffusion of atoms by annealing.

The grains of the P sample are found to be uniform with average grain size of 27 nm while for $A_{400}$, $IA_{400}$ sample the grains are randomly distributed with average grain size of ~41 nm and ~48 nm, respectively. The grains in $IA_{400}$ samples were observed to be agglomerated under disorder induced by SHI which resulted in the formation of hills and valleys due to diffusion and migration of surface particles. These agglomeration of grains are seen as coral like structure in the SEM images (figure 7(c)) of the same sample.

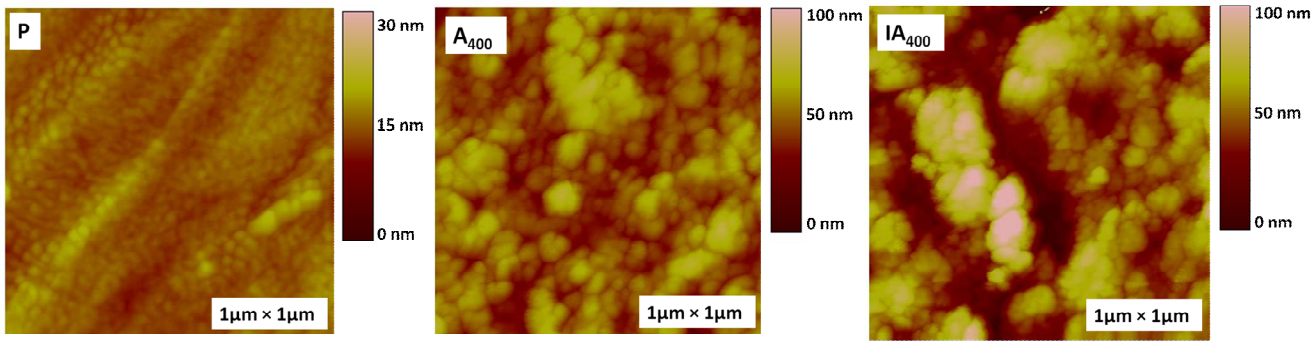


(a) (b) (c)

Figure 8: AFM images of (a) P, (b) $A_{400}$ (c) $IA_{400}$ sample

**Electrical and Transport Measurement**

Figure 9(a) shows the thermoelectric power in the temperature range of 300 K to 420 K for P, $IA_{200}$, $IA_{300}$ and $IA_{400}$ Co/Sb thin films. In the case of P sample, Sb is present on the top layer and its thickness is 3 times greater than the well separated Co layer. Therefore, the thermoelectric power of P sample is mainly determined by the thermoelectric power of Sb layer[37]. Thermoelectric power of IA sample is found to be higher than the P sample at 420 K and further it increases with the increase in post annealing temperature. Figure 9(b) shows a comparison of the effect of annealing at 400$^{o}$C on thermoelectric power of pristine and irradiated samples. The measured thermoelectric power at 420 K for P, $A_{400}$ and $IA_{400}$ Co/Sb film are ~6, ~ 7 and ~ 9.5 μV/K respectively (with an error of ±0.5μV/K)[18]. The thermoelectric powers of $IA_{400}$ and $A_{400}$ thin films are found to be 58% and 16% higher than the P sample, respectively. The thermoelectric power of $IA_{400}$ sample are found to be ~35 % greater than the $A_{400}$ sample. The increase in the value of thermoelectric power of $A_{400}$ and $IA_{400}$ Co/Sb thin film in comparison to the P sample is due to the evolution of different phases of CoSb alloy. In case of $A_{400}$ sample CoSb, $CoSb_2$ and $CoSb_3$ phases are formed while in $IA_{400}$ sample only $CoSb_2$ and $CoSb_3$ phases are observed. $CoSb_3$ being a skutterudite material have the best thermoelectric material among all Co-Sb alloys. In case of $IA_{400}$ sample concentration of $CoSb_3$ phase is found to be 17% higher than in $A_{400}$ sample, therefore the thermoelectric power of $IA_{400}$ sample is found to be higher than the $A_{400}$ samples at 420K. When one compares these values with the studies of Co-Sb thin films (400-600nm) prepared by co-sputtering of Co and Sb, the thermoelectric power ranges from 2μV/K to 15μV/K for Sb~65% forming $CoSb_2$ phase and 1μV/K to 80μV/K for Sb~76% forming $CoSb_3$ phase in the temperature range of 300 to 400 K[9]. In the present case the post irradiated annealed sample $IA_{400}$ (~177nm) prepared by ion beam induced mixing have Sb~53% and the thermoelectric power measured in the temperature range of 300-420K varies from 3μV/K to 10μV/K. The thermoelectric power of $IA_{400}$ sample prepared by ion beam induced mixing is quite smaller than the sample prepared by co-deposition, this might be because of smaller thickness of $IA_{400}$ sample which is nearly 1/2 or 1/3 times smaller than the co-deposited sample. Though the values of thermoelectric power measured in the temperature range 300-420K is small in number but there is a significant increase in the slope of the $IA_{400}$ sample having maximum $CoSb_3$ components, which suggests that the sample will have remarkable improvement at higher

temperature around 700K where it is known to have best thermoelectric power. This is the first study on thermoelectric properties of $CoSb_3$ thin film prepared by ion beam induced mixing. It is expected that the damage produced by ion beam irradiation in the IA samples will have lower lattice thermal conductivity than the A sample due to phonon scattering by the defects created.

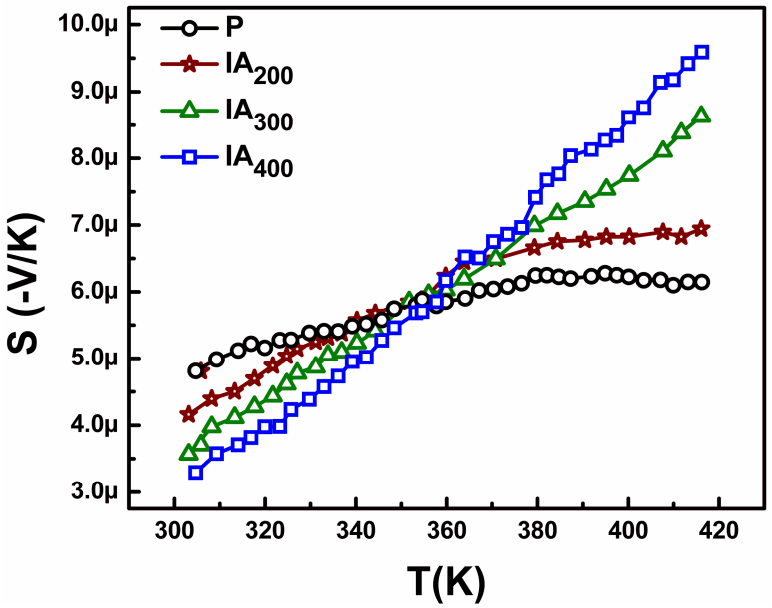


**(a)**

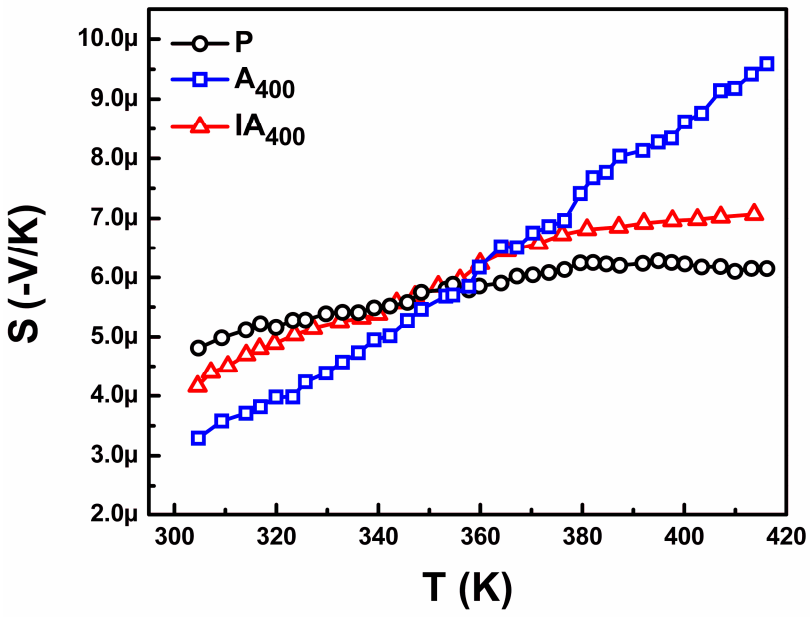


**(b)**

Figure 9. Thermoelectric power in the temperature range of 300 to 420K of (a) P, $IA_{200}$, $IA_{300}$ and $IA_{400}$ Co/Sb bilayer thin film (b) P, $A_{400}$ and $IA_{400}$ Co/Sb bilayer thin film. $IA_{400}$ have thermoelectric power higher than P and $A_{400}$.

The temperature dependence of the electrical resistivity (ρ) in the temperature range of 300K to 420K for the P, $IA_{200}$, $IA_{300}$ and $IA_{400}$ thin films are shown in Figure 10(a). The electrical resistivity decreases with temperature showing the metallic behavior for all the films. The slope of resistivity curve increases for the irradiated post annealed films in comparison to the P thin film. Further the slope of resistivity increases with post annealing temperature of IA sample from 200°C to 400°C. Figure 10(b) shows a comparison between the effect of annealing at 400°C on resistivity of unirradiated and irradiated thin film samples. The slope of $IA_{400}$ sample is found to be more than the $A_{400}$ sample. The temperature coefficient of resistance,

$\alpha=\Delta R/(R_0\times\Delta T)$ calculated for P, $A_{400}$, and $IA_{400}$ sample were found to be $6.64\times10^{-4}$, $19.01\times10^{-4}$ and $27.01\times10^{-4}$ $K^{-1}$ . $IA_{400}$ thin film sample shows low electrical resistivity compared to $A_{400}$ sample at room temperature. The low thermoelectric power of $IA_{400}$ sample at room temperature is a consequence of its low resistivity at room temperature and it increases with the temperature up to 420K.

Table 2 shows Hall measurements of the thin films of P, $A_{400}$, and $IA_{400}$ at room temperature using a magnet field of 0.57 T. The Hall coefficients of all three samples are negative, indicating *n*-type conduction at room temperature. The carrier concentration for P, $A_{400}$, and $IA_{400}$ was found to be $4.97\times10^{18}$, $11.1\times10^{18}$, and $84.5\times10^{18}$ $cm^{-3}$ respectively. As evident from table 2, in case of $IA_{400}$ sample, both carrier concentration and mobility are higher at room temperature in comparison to $A_{400}$ sample leading to decrease in electrical resistivity ($\rho=1/ne\mu$) of $IA_{400}$ sample. It is known that ion irradiation increases resistivity of a material due to defect creation. Despite of ion irradiation, the $IA_{400}$ sample exhibits low electrical resistivity, which could be due to the higher carrier concentration and mobility of the $IA_{400}$ sample as a result of agglomeration of grains evident from the SEM and AFM results which provide a continuous path for charge carrier transport. These results are found to be in accordance with the work reported by Zheng *et al*[38]. They prepared In filled $CoSb_3$ thin films using magnetron sputtering and found that both the electrical conductivity and the Seebeck coefficient of the thin films increase with grain size after

filling In. In addition Khan *et al.*[39] synthesized $CoSb_3$ compounds using chemical alloying method and showed the dependence of conductivity on grain size. Samples with smaller grains contain more grain boundaries that scatter electrons lightly and therefore cause slight reduction of electrical conductivity, or increase of electrical resistivity.

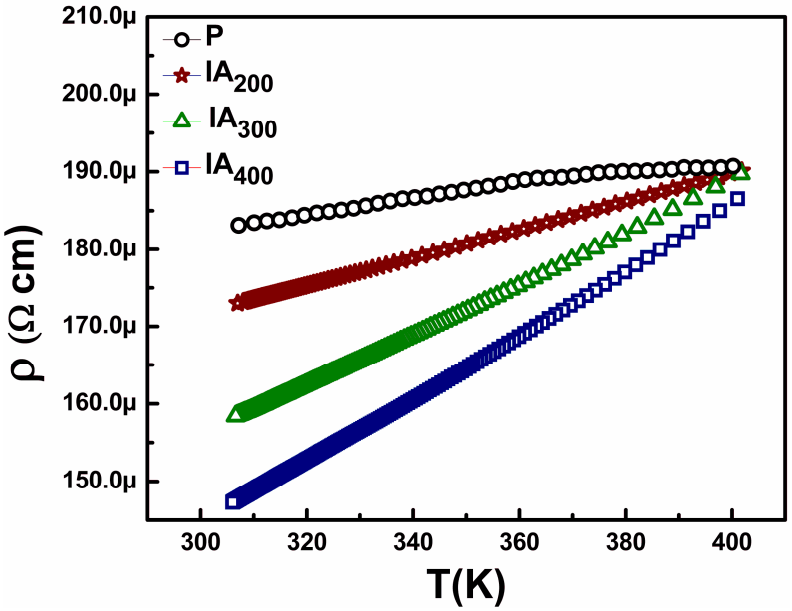


**(a)**

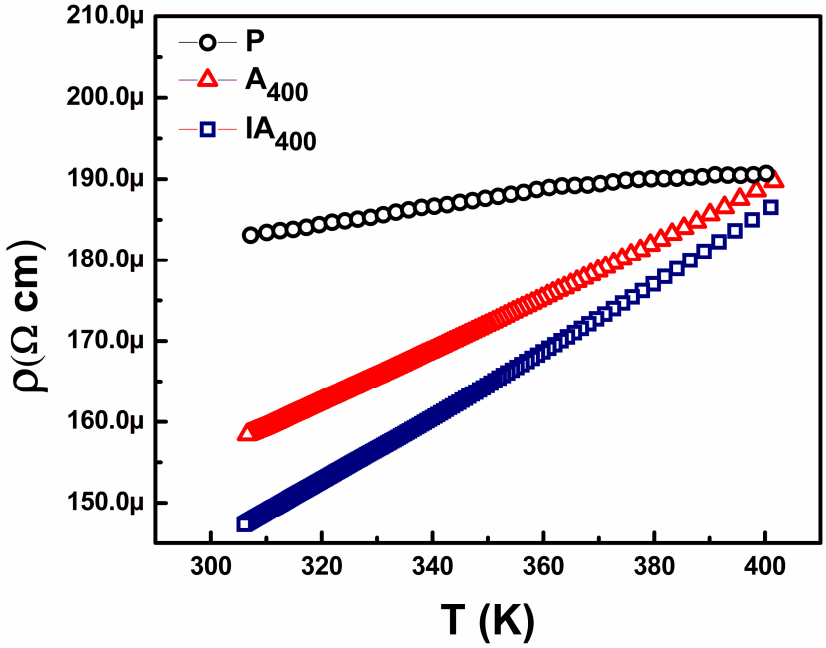

**(b)**

Figure 10: Resistivity in temperature range of 300 to 420K of Co/Sb bilayer thin film (a) P, $IA_{200}$, $IA_{300}$, and $IA_{400}$ (b) P, $A_{400}$ and $IA_{400}$.

Table 2: Comparison of some electrical properties of the P, $A_{400}$ and $IA_{400}$ samples.

| | **Carrier Concentration ($cm^{-3}$)** | **Hall Mobility ($cm^2/Vs$)** | **Electrical resistivity (Ωcm)** |
|---|---|---|---|
| **Pristine (P)** | $4.97\times10^{18}$ | 33.81 | $183\times10^{-6}$ |
| **Annealed ($A_{400}$)** | $11.1\times10^{18}$ | 2.53 | $159\times10^{-6}$ |
| **Irradiated post Annealed ($IA_{400}$)** | $84.5\times10^{18}$ | 7.45 | $146\times10^{-6}$ |

The physical mechanism responsible for thermoelectric power enhancement is understood based on the phase evolution caused by the ion beam induced mixing. SHI on its passage through a material predominantly deposits a large amount of energy in the electronic subsystem of the material creating point defects (vacancies and interstitial atoms). In case of a bilayer system if the defects created by ion beam are mobile, it causes diffusion of the atoms of the solid across the interface resulting in ion beam mixing. When the mobility of defects is low, these defects remain locally and cause no diffusion. The *ex-situ* heat treatment to these irradiated material during annealing provides sufficient energy to the system to enhance the atomic mobility through these defects, and across the interface leading to the uniform mixing of the two layers, this phenomenon is known as radiation induced mixing and it is schematically shown in figure 11.

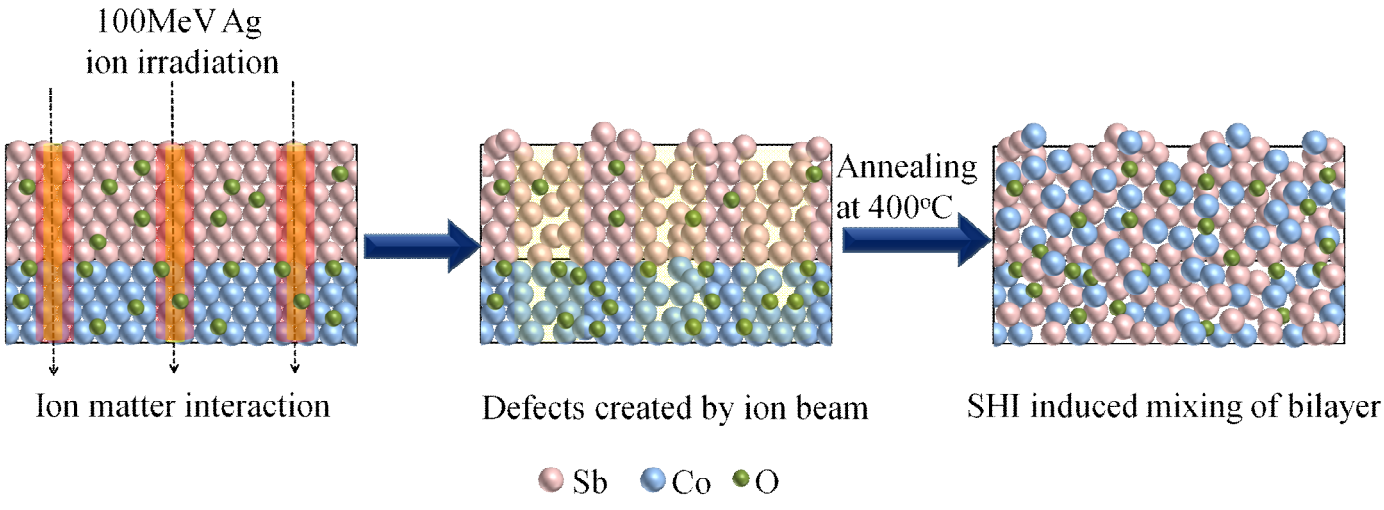

Figure 11: Schematic diagram demonstrating mechanism of ion beam induced mixing. SHI creates immobile material defects via ion-matter interaction which enhances mixing when thermal energy is supplied during annealing process.

Through RUMP simulation it was quantitatively estimated that within the interfacial (mixed) zone in the A and IA sample, the number of Co and Sb atoms are also not uniformly distributed. This implies that the formation of mixed phases. The interdiffusion that takes place across the interface in SHI irradiated sample increases with the post annealing temperature due to increase in mobility of atoms with temperature (figure 1). The phenomenon of ion beam induced mixing on post annealing results in higher and uniform mixing in comparison to the mixing by thermal annealing at the same temperature and for same duration (figure 3). Depth profiling of RBS data shows that annealing had caused incorporation of small amount of oxygen in the samples. Oxygen incorporated in the sample either at the interface or diffused through the sample during annealing can act as a barrier to retard CoSbx growth. Therefore, the role of SHI irradiation may be summarized as being responsible for dispersing any diffusion barrier presented by oxygen in the samples and, creation of point defects in Co/Sb. Heat treatment of the irradiated sample provided ion generated defects with the necessary migration energy to cross the interface, produce mixing effects and enhance compound formation.

HRXRD figure 4(a-b) gives the crystalline phases formed after annealing the SHI irradiated and unirradiated sample at 400$^{o}$C. A combination of CoSb, $CoSb_2$, $CoSb_3$ with a small amount of $Sb_2O_3$ phase are evolved in A400 and in IA400 sample only $CoSb_3$ and $CoSb_2$ phase is seen. Co-Sb phase is obtained in SHI irradiated samples at much lower post irradiation annealing temperatures (300$^{o}$C), compared to the pristine films with thermal annealing (400$^{o}$C).

SHI irradiation modifies the surface morphology of the sample and it is found that the grains of $IA_{400}$ sample are agglomerated and form a coral like structure in analogy to that of $A_{400}$ sample. The connected grains in IA400 provide a continuous path for the motion of charge carriers, resulting in higher mobility of the carriers through the sample. The increase in grain size and carrier concentration in $IA_{400}$ sample has cooperatively reduced the electrical resistivity in comparison to A400 sample. In contrast the thermoelectric power of IA400 sample enhances in comparison to A400 sample due to evolution of 17% greater concentration of $CoSb_3$ compound in the homogeneously mixed layer of IA400 sample.

## Conclusion

The SHI induced mixing is one of the experimental methods for the synthesis of $CoSb_3$ phase on post irradiation annealing of Co/Sb bilayer thin film. A comparative study of unirradiated and irradiated Co/Sb bilayer at same annealing temperature showed that higher mixing take place for the irradiated post annealed sample. XRD measurement showed that in case of $IA_{400}$, the composition of $CoSb_3$ is much higher than in $A_{400}$ sample, RAMAN spectroscopy also confirmed the formation of Co-Sb alloy. SEM and AFM images showed a change in surface morphology for both the $A_{400}$ and $IA_{400}$ sample with appearance of grain agglomeration in the irradiated post annealed sample. The thermoelectric measurements showed that $IA_{400}$ have higher thermoelectric power than the $A_{400}$ sample at same temperature due to the presence of higher concentration of $CoSb_3$ phase in case of $IA_{400}$ sample.

## ACKNOWLEDGEMENT

One of the authors (Manju Bala) is grateful to the Council for Scientific and Industrial Research (CSIR) for providing financial support in the form of fellowship. The authors are grateful to the Department of Science and Technology (New Delhi) for providing the SEM under the Nano Mission Project and XRD system at IUAC under the IRHPA project to boost the research activities. The authors would like to thank Mrs. Indra Sulania, Dr. Saif A Khan, Mr.Sunil Ojha, Subodh Gautam, Dr. Pawan K. Kulriya for their help in various analysis and discussion. Author also thank Saha Institute of Nuclear Physics, India for facilitating the XRD experiment at the Indian Beamline, Photon Factory, KEK, Japan.

## Reference

1. J. Wolfenstine, D. Tran, K. Zhou and J. Sakamoto, *Thermoelectric Properties of Cobalt Triantimonide (CoSb3) Prepared by an Electrochemical Technique*, DTIC Document, 2010.
2. M. Rull-Bravo, A. Moure, J. Fernández and M. Martín-González, *RSC Advances*, 2015, 5, 41653-41667.
3. J. Zhang, Q. Lu, K. Liu, L. Zhang and M. Zhou, *Materials Letters*, 2004, 58, 1981-1984.

4. G. J. Snyder and E. S. Toberer, *Nature materials*, 2008, 7, 105-114.
5. V. Keppens, D. Mandrus, B. Sales, B. Chakoumakos, P. Dai, R. Coldea, M. Maple, D. Gajewski, E. Freeman and S. Bennington, *Nature*, 1998, 395, 876-878.
6. M. M. Koza, M. R. Johnson, R. Viennois, H. Mutka, L. Girard and D. Ravot, *Nature Materials*, 2008, 7, 805-810.
7. J. Sharp, E. Jones, R. Williams, P. Martin and B. Sales, *Journal of applied physics*, 1995, 78, 1013-1018.
8. K. Wojciechowski, *Materiały Ceramiczne*, 2010, 62, 461-464.
9. A. Ahmed and S. Han, *Thin Solid Films*, 2015, 587, 150-155.
10. V. Savchuk, A. Boulouz, S. Chakraborty, J. Schumann and H. Vinzelberg, *Journal of applied physics*, 2002, 92, 5319-5326.
11. S. Sarath Kumar, A. Alyamani, J. Graff, T. Tritt and H. Alshareef, *Journal of Materials Research*, 2011, 26, 1836-1841.
12. M. Daniel, C. Brombacher, G. Beddies, N. Jöhrmann, M. Hietschold, D. Johnson, Z. Aabdin, N. Peranio, O. Eibl and M. Albrecht, *Journal of Alloys and Compounds*, 2015, 624, 216-225.
13. J. Dong, K. Yang, B. Xu, L. Zhang, Q. Zhang and Y. Tian, *Journal of Alloys and Compounds*, 2015, 647, 295-302.
14. S. Gupta, D. Agarwal, S. Khan, S. Neeleshwar, S. Ojha, S. Srivastava, A. Tripathi, S. Amirthapandian, B. Panigrahi and D. Avasthi, *Materials Science and Engineering: B*, 2014, 184, 58-66.
15. A. Ibrahim and D. Thompson, *Nuclear Instruments and Methods in Physics Research Section B: Beam Interactions with Materials and Atoms*, 1985, 7, 566-570.
16. R. Benenson, V. Tikku, D. Kollewe and H.-S. Jin, *Nuclear Instruments and Methods in Physics Research*, 1983, 209, 185-189.
17. A. Gupta, *Vacuum*, 2000, 58, 16-32.
18. P. Dhuri, A. Gupta, S. Chaudhari, D. Phase and D. Avasthi, *Nuclear Instruments and Methods in Physics Research Section B: Beam Interactions with Materials and Atoms*, 1999, 156, 148-152.
19. I. Kasko, C. Dehm, L. Frey and H. Ryssel, *Nuclear Instruments and Methods in Physics Research Section B: Beam Interactions with Materials and Atoms*, 1993, 80, 786-789.
20. D. Bhattacharya, S. Srivastava, P. Sahoo, G. Principi, D. Kabiraj, T. Som, V. Kulkarni and D. Avasthi, *Surface and Coatings Technology*, 2002, 158, 59-63.
21. L. Hicks, T. Harman, X. Sun and M. Dresselhaus, *Physical Review B*, 1996, 53, R10493.
22. R. Venkatasubramanian, E. Siivola, T. Colpitts and B. O'quinn, *Nature*, 2001, 413, 597-602.
23. S. Gupta, D. Agarwal, S. Tripathi, A. Tripathi, S. Neeleshwar and D. Avasthi, *Applied Surface Science*, 2013, 265, 124-129.
24. A. I. Hochbaum, R. Chen, R. D. Delgado, W. Liang, E. C. Garnett, M. Najarian, A. Majumdar and P. Yang, *Nature*, 2008, 451, 163-167.
25. M. Bala, S. Gupta, T. S. Tripathi, S. Varma, S. K. Tripathi, K. Asokan and D. K. Avasthi, *RSC Advances*, 2015, 5, 25887-25895.
26. T. L. Alford, L. C. Feldman and J. W. Mayer, *Fundamentals of nanoscale film analysis*, Springer Science & Business Media, 2007.
27. T. Tripathi, M. Bala and K. Asokan, *Review of Scientific Instruments*, 2014, 85, 085115.
28. D. Zeng, C. Xie, B. Zhu and W. Song, *Materials Letters*, 2004, 58, 312-315.
29. O. Degtyareva, V. V. Struzhkin and R. J. Hemley, *Solid state communications*, 2007, 141, 164-167.
30. X. Su, H. Li, G. Wang, H. Chi, X. Zhou, X. Tang, Q. Zhang and C. Uher, *Chemistry of Materials*, 2011, 23, 2948-2955.
31. G. Nolas, C. Kendziora and H. Takizawa, *Journal of applied physics*, 2003, 94, 7440-7444.

32. Y. S. Chaudhary, S. A. Khan, R. Shrivastav, V. R. Satsangi, S. Prakash, D. Avasthi and S. Dass, *Nuclear Instruments and Methods in Physics Research Section B: Beam Interactions with Materials and Atoms*, 2004, 225, 291-296.
33. D. Mohanta, N. Mishra and A. Choudhury, *Materials Letters*, 2004, 58, 3694-3699.
34. S. Chandramohan, R. Sathyamoorthy, P. Sudhagar, D. Kanjilal, D. Kabiraj and K. Asokan, *Nuclear Instruments and Methods in Physics Research Section B: Beam Interactions with Materials and Atoms*, 2007, 254, 236-242.
35. N. Tigau, V. Ciupina and G. Prodan, *Journal of Optoelectronics and Advanced Materials*, 2006, 8, 37.
36. J. Sofo and G. Mahan, *Physical Review B*, 1998, 58, 15620.
37. A. Boyer, D. Deschacht and E. Groubert, *Thin Solid Films*, 1981, 76, 119-128.
38. Z.-h. Zheng, P. Fan, Y. Zhang, J.-t. Luo, Y. Huang and G.-x. Liang, *Journal of Alloys and Compounds*, 2015, 639, 74-78.
39. A. Khan, M. Saleemi, M. Johnsson, L. Han, N. Nong, M. Muhammed and M. S. Toprak, *Journal of Alloys and Compounds*, 2014, 612, 293-300.


## Graphical Abstract

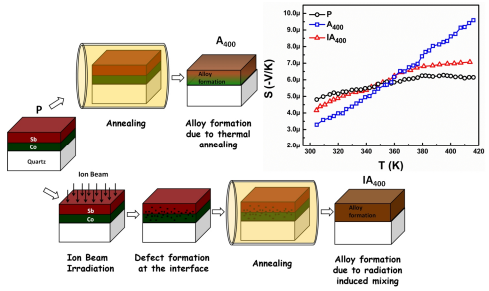


Thermoelectric power enhancement of ion beam synthesized Co-Sb alloy thin film.